Published in final edited form as:
*Adv Healthc Mater*. 2014 November ; 3(11): 1753–1758. doi:10.1002/adhm.201300678.

# Confinement and Deformation of Single Cells and Their Nuclei Inside Size-Adapted Microtubes

**Britta Koch Dr.**,
Institute for Integrative Nanosciences IFW Dresden, Helmholtzstraße 20 Dresden, D-01069, Germany

**Samuel Sanchez Dr.**[*,[+]],
Institute for Integrative Nanosciences IFW Dresden, Helmholtzstraße 20 Dresden, D-01069, Germany

**Christine K. Schmidt Dr.**[*],
The Gurdon Institute and Department of Biochemistry University of Cambridge Tennis Court Road Cambridge, CB2 1QN, UK

**Anka Swiersy Dr.**,
Institute for Integrative Nanosciences IFW Dresden, Helmholtzstraße 20 Dresden, D-01069, Germany; Klinik und Poliklinik für Viszeral-Thorax- und Gefäßchirurgie Universitätsklinikum Carl Gustav Carus Fetscherstraße 74, Dresden, D-01307, Germany

**Stephen P. Jackson Prof.**, and
The Gurdon Institute and Department of Biochemistry University of Cambridge Tennis Court Road Cambridge, CB2 1QN, UK; The Wellcome Trust Sanger Institute, Hinxton Cambridge, CB10 1SA, UK

**Oliver G. Schmidt Prof.**
Institute for Integrative Nanosciences IFW Dresden, Helmholtzstraße 20 Dresden, D-01069, Germany; Material Systems for Nanoelectronics Chemnitz University of Technology Reichenhainer Str. 70 Chemnitz, D-09107, Germany

The mechanical properties of the microenvironment of cells, like substrate rigidity and topography, have a considerable impact on various aspects of cell fate, such as proliferation, [1–3] apoptosis,[4] and differentiation.[5,6] For example, on 2D predefined adhesion sites, the cells need a minimum area for spreading to survive[4] and asymmetrical patterns manipulate cell orientation during mitosis.[3] Human mesenchymal stem cells cultured on a nanograting respond to the nanotopographical cues through a significant extension of the cell nucleus along the axis of the grating.[7] Human embryonic and mesenchymal stem cells that orient along nanopatterned groves and ridges are promoted to



[*]sanchez@is.mpg.decs681@cam.ac.uk.
[+]Present address: Dr. S. Sanchez, Max Planck Institute for Intelligent Systems, Heisenbergstr. 3, Stuttgart D-70569, Germany

**Supporting Information** Supporting Information is available from the Wiley Online Library or from the author.

differentiate preferentially along the neural lineage so that the topographic features of the substrate not only induce the differentiation process but also affect the specific functions of the resulting cells.[5,6]

The mechanisms by which physical cues impact cell functioning are just starting to be unraveled[8] and their investigation is complicated by the 3D character of physiological tissues, which is challenging to recapitulate in vitro.[9] 3D cell culturing scaffolds are therefore of particular interest for in vitro tissue engineering applications because they mimic the 3D aspects of the in vivo extracellular environment in contrast to the traditional and frequently used monolayer cell culture approach. Examples are fiber meshworks, sponges, and hydrogels of several biocompatible materials.[10,11] The analysis of cells grown inside these structures shows that the physical properties of the 3D matrices evoke a cell response that differs from the one on 2D substrates, such as morphology changes[10,12] and the formation of modified adhesion complexes.[13]

It is the subject of current research how cells transform the physical properties of their microenvironments into a biochemical response, a process termed mechanotransduction.[14,15] The investigation of the responses that the cells generate by a continuous probing and sensing of the environment has been facilitated by the emergence of microtechnologies.[16,17] Advanced microfabrication methods have enabled the reproducible and parallel fabrication of patterned cell culture scaffolds by selectively controlling and manipulating the mechanical features of the substrate.[12]

A non-invasive shape change of cells can, for example, be achieved by the topographical patterning of the cell culture substrates with micro-sized adhesion areas[8,18,19] or microgrooves.[15] These micropatterned substrates allow for the analysis of single cells by, for example, microscopic means.[15,19,20] The observed morphology change of the attached cells has been shown to influence the shape of the cell nucleus and to impact cell functioning. There is, for instance, accumulating evidence that changes in the morphology of the cell nucleus can influence its gene expression pattern by affecting the non-random positioning of chromosomes.[8,15,18,21–23]

However, the fabrication of topographically structured substrates that can confine cells in more than one dimensionality remains challenging. The usage of 3D biomaterials scaffolds suffers the drawback of decreased single-cell resolution due to the increased volume depth, while microstructured substrates usually provide an asymmetric polarization of matrix adhesions at the basal side of the cell. A suitable technique that circumvents these restrictions is rolled-up nanotechnology on polymers,[24] which can generate transparent and biocompatible silicon oxide/silicon dioxide ($SiO/SiO_2$) microtubes with different diameters that readily serve as cell culturing scaffolds. Inside the microtubes, cell growth is restricted in two dimensions (lateral and vertical) while the behavior of single cells can be easily observed. These microctubes have been shown to support the growth of various types of cells such as yeast[25] and HeLa cells,[26] as well as guide neuron extensions (e.g. axons),[27] and have been successfully employed to study mitotic processes in confined spaces.[28]

Here, we report the confinement and microscopic analysis of single human osteosarcoma U2OS cells growing inside tailor-made microtubes. The aim is to study the effects of varying extents of spatial confinement, given by biofunctionalized silicon oxide (glass) microtubes, on different cell characteristics. Specifically, we employed the microtube system to investigate the effects of constricted cell growth on the morphology and integrity of the cell nucleus, the stiffest and largest organelle of the cell, and on two geometrically demanding processes—cell growth and cell division. We show that the U2OS cells were successfully confined inside the transparent structures. Depending on the tube diameter as a measure of the confinement level, we observed a distinct cell elongation that strongly affected the morphology of the cell nucleus. By quantifying the amount of DNA damage foci present in the cells, we found no correlation with the size of the confining structures indicating that the changes in nuclear morphology had no major effects on nuclear DNA integrity. In contrast, while the confined cells were able to divide inside microtubes of a wide diameter range, the majority of cells did not survive mitosis (cell division) inside the smallest diameter range of microtubes. Collectively, these findings demonstrate the applicability of the rolled-up microtubes as versatile, 3D biocompatible, and adjustable cell culturing scaffolds for various materials–cell investigations while mimicking the in vivo confinement of cells in their physiological 3D environment.

To assess the effects of varying levels of spatial confinement on cellular shape and integrity, we tuned the diameters of the microtubes during the fabrication process [29] and adjusted them to fit the sizes of U2OS cells and their cell nuclei (see Figure 1a). We determined the nuclear dimensions of freely growing U2OS cells to be 16 ± 2 μm in width, 23 ± 3 μm in length, and 4 ± 1 μm in height ($n$ = 60). Therefore, we fabricated different $SiO/SiO_2$ scaffolds with microtube diameters ranging from 4 μm (the average nucleus height of free growing cells) to 25 μm (a little larger than the average nucleus length of free growing cells). This range was chosen to ensure a significant confinement of cells that grow inside microtubes of smaller diameters as well as not significantly constricting the cells inside microtubes of larger diameters. A biofunctionalization step of the sample surface with fibronectin, a protein of the in vivo extracellular matrix, promoted cell growth on the silicon oxide substrate and inside the microtubes. U2OS cells were seeded onto each sample at high density to maximize the number of cells migrating into the microtubes within 2 d of incubation. The optical transparency of the silicon oxide material of the microtubes enabled the high-resolution microscopic observation of single cells, which entered the microtubes and grew inside the $SiO/SiO_2$ scaffolds. A representative movie that demonstrates how the U2OS cells first extended cell membrane outgrowths into the microtube, before translocating the main cell body into the structure, is provided in the Supporting Information (see Movie S1).

The imaging of the samples demonstrated that the cells were able to grow and survive inside the confinement for a wide range of microtube sizes down to a minimum diameter of 5 μm (see Figure 1), below which the tubes did not sustain cell growth anymore. Fixation of the cells, staining of the DNA by DAPI and bright-field microscopy, as well as fluorescence imaging, revealed the shape change of the cell nucleus in dependence on the microtube diameter. In order to quantify this effect, we acquired $z$-stacks (image series of different

focal planes) of confocal images at the positions of interest with a Zeiss LSM 700 inverted microscope. The widths and lengths of the cell nuclei were measured using the maximum intensity projections of each *z*-stack. The nucleus length was defined as the longest dimension of the DAPI-stained area, the nucleus width as the widest dilation orthogonally to it. The cut view of the *z*-stack projection then revealed the average nuclear heights (see Figure 1 b,c). By forming the nuclear aspect ratios (nucleus length over width and nucleus length over height, see Figure 1d), we accounted for any differences in nuclear volumes that arise from the progression through the cell cycle for instance due to increased protein and DNA synthesis in preparation for mitosis.[30]

Strikingly, the nuclear aspect ratios revealed two microtube diameter ranges, which show different effects on the nuclear dimensions. For diameters ranging from 17 to 8 μm, the aspect ratios increased only slightly with decreasing microtube diameters, implying that the cells adapted to the reduction in available space without a profound effect on nuclear shape.

The cell nucleus height and length remained fairly constant in this microtube diameter range, while the nucleus width slightly decreased with decreasing microtube diameter (data provided in Table S1 and depicted in Figure S1, Supporting Information).

At a tube diameter of 8 μm the aspect ratios of the nuclear width and height reached identical values reflecting an elongated, rod-like shaped nucleus, which is in sharp contrast to the rather flat and spread-out morphology of unconfined U2OS cell nuclei. For microtubes smaller than this 8 μm threshold, the dependence of the aspect ratios on the microtube diameter became prominent. Any reduction of the microtube diameter below this threshold resulted in a linear and equal decrease of the nucleus width and height from 6 ± 1 to 4 ± 1 μm (see Table S1, Supporting Information) while the nucleus length increased to compensate for the restriction and to conserve the volume of the cell nucleus.

When compared to free growing cells, it becomes evident that the U2OS cells inside the microtubes possessed nuclei that were generally more slender and not as flat as the cells on the planar substrate. The narrowed shape of the cell arises due to the lateral restriction of the cell dilation by the microtube wall. Surprisingly, the nucleus height was substantially increased inside the microtubes, which cannot only be accounted for by the 2D confinement, as the cell nuclei dimensions were hardly affected in the microtube diameter range from 8 to 17 μm. The functionalized microtubes offer a cell culture environment where the cells can form adhesions to the substrate all around the cell body so that a transition from a planar and spread to a more 3D morphology occurs. The dimensions of the cell nuclei were therefore directly influenced by the increased dimensionality of the cell culture scaffold. In microtubes with diameters smaller than 8 μm, the cells have to elongate profoundly to be able to squeeze into the microtube. The decrease of the nucleus width and height below a value of 6 ± 1 μm can only be compensated for by a considerable increase of the nucleus length indicating a significant remodeling of the cell nucleus content.

These results are in line with the recent finding that the nucleus is a large cell organelle that can undergo remarkable deformation to migrate through small pores in 3D scaffolds. It is assumed that the changes in the nuclear shape are transient and reflect the interplay of forces

imposed by the geometry of the cell environment and the intracellular counterforces.[31] Therefore, the microtube cell culture scaffold is suitable to determine the spatial limit for the "self-imposed" nuclear deformation of cells. This spatial limit for U2OS cells can be found at around 4 μm, as these cells do not readily grow into microtubes of this or smaller diameters. This corresponds to the fact that the confinement inside these small microtubes would force both the widths and the heights of the confined nuclei to acquire values lower than the average 4 μm height of nuclei in U2OS cells grown on planar substrates.

Next, we evaluated if the observed changes in nuclear morphology, especially inside the narrowest microtubes below 8 μm, could influence the integrity of DNA, which is tightly packed and harbored inside the nucleus to protect and maintain genome stability. To do so, we used GFP-53BP1 U2OS cells[32] that were modi fied to stably express a fluorescently labeled marker of the DNA damage response pathway (p53-binding protein 1, 53BP1).[33] We quantified the numbers of GFP-53BP1 fluorescence foci (spots of higher light intensity) inside the U2OS nuclei as markers of DNA lesions to assess the amount of DNA damage depending on the diameter of the microtube (see Figure 2). We detected no correlation between the two parameters (compare Figure 2a with b–d and see Figure 2e) demonstrating that the quantity of DNA lesions in asynchronous cell cultures was overall comparable between confined and freely growing cells. However, at this stage, we cannot exclude that certain changes in DNA integrity may still occur in selected cell cycle stages. This finding confirms the applicability of the microtube structures as cell culturing scaffolds that can directly manipulate the shape of whole cells and their nuclei without grossly affecting the integrity of DNA even when the cells are grown inside the narrowest microtubes of diameters between 5 and 8 μm.

To assess whether the tubes impacted on the fate of U2OS cells, for instance, by affecting their growth and proliferation—two processes that depend on nuclear function—we studied the occurrence of mitosis and the survival of U2OS cells in microtubes of varying diameters (see Figure 3a,b). We performed live-cell imaging experiments for at least 20 h on cells grown either on planar surfaces (reference cells) or inside differently sized microtubes to analyze the survival rates of confined and unconfined cells. Cells undergoing apoptosis were clearly discriminable due to extensive blebbing and dissolution of the GFP-BP1 fluorescence signal from the cell nucleus. The majority of cells (80%, Figure 3c) survived throughout the observation period in microtubes of diameters larger than 8 μm, compared to almost 100% in unconfined conditions. This behavior changed considerably for cells that grew in microtubes with diameters smaller than 8 μm where half of the cells died.

One process that could affect the survival of cells under confinement is mitosis. We therefore discriminated in our analysis between dividing and non-dividing cells and kept monitoring the cell fate of any arising daughter cells for an additional time period of at least 3.5 h after mitosis (Figure 3d). The analysis revealed that around half of the cells underwent a first mitotic event within the observation period in both unconfined cells and cells grown inside microtubes >8 μm (total heights of left bars in Figure 3d). However, an increased proportion of the cells died inside microtubes >8 μm (hatched and striped bar fractions in Figure 3d) and more cells died after the occurrence of mitosis than without a cell division inside microtubes of this range. Still, one third of the confined cells were able to divide and

Europe PMC Funders Author Manuscripts

survive inside confinements with a minimum diameter of 8 μm compared to 53% in free cells. In contrast, only 18% of the cells confined in tubes <8 μm divided and half of these died in the 3.5 h after mitosis allowing only 9% of the daughter cells to survive mitosis inside these highly constricting cavities.

In summary, although the cells and their nuclei elongate and adopt the shape of the topographic structures, the entry of cells into mitosis and the long-time survival of the confined cells are affected. Moreover, while cells are flexible and can adjust to a topographic confinement to some extent,[34–37] our findings demonstrate that they require a minimum space for survival and division. We conclude that extended confinement and substantial squeezing of the cell nucleus can impair the normal progression of the cell cycle.

Hence, our results demonstrate that the microtube structures serve as versatile and biocompatible 3D cell culturing scaffolds. Their dimensions are designed during the fabrication process to confine and to noticeably change the cell shape and hence the morphology of the cell nucleus. The on-chip glass microtubes serve as an easily controllable tool to mechanically manipulate single cells and to test the maximum deformability of their nuclei without grossly perturbing the integrity of their DNA. The tunability of the microtube diameters allows for the adaption of the confinement to the specific cell type under investigation. The microtube cell culture system can be further employed to study the dynamics of cell nucleus deformation and remodeling, as well as the effect of a defined and long-term nucleus deformation on various cell responses. Examples are changes in chromosome positioning and protein expression levels. Another interesting follow-up study could investigate the influence of the biofunctionalization on the cell response to the increased dimensionality of the cell culture system by substituting fibronectin with other proteins of the native extracellular matrix environment. Taken together, these and further investigations using the microtube cell culturing system described above will help increase our understanding of the molecular processes involved in the mechanotransduction of extracellular signals within the 3D spatial and mechanical configuration of tissues.

## Experimental Section

### Microtube Sample Fabrication

The fabrication of the transparent silicon monoxide/silicon dioxide ($SiO/SiO_2$) microtube samples is described in detail elsewhere.[24,29] Briefly, a layer of ARP-3510 photoresist (Allresist GmbH) was spincoated at 3500 rpm on 18 mm × 18 mm cover glass substrates (high-performance, thickness no. 1½, Zeiss). The polymer film was patterned by conventional photolithography to produce squares of 100 μm in width and of a length varying between 100 and 500 μm. For the creation of the $SiO/SiO_2$ bilayer film 5 nm of SiO and between 20 and 100 nm of $SiO_2$ are then deposited in a 30° glancing angle electron beam deposition step at deposition rates of 5 or 0.5 Å $s^{-1}$, respectively. The glancing angle ensures the maintenance of an uncovered region behind the polymer squares (ballistic shadow effect). This window defines the starting point for the selective dissolving of the photoresist film in dimethyl sulfoxide (Sigma–Aldrich) so that the gradual release of the prestressed silicon oxide film leads to the self-assembly of the rolled-up microtube structures. The samples were subsequently dried by critical point drying (CPD 030 Critical

Point Dryer, Bal-Tec AG) and coated with an 18-nm thick aluminum oxide ($Al_2O_3$) film by atomic layer deposition (Savannah 100, Cambridge NanoTech Inc.) to avoid the collapse of the thin structures. The cover slides were then functionalized with fibronectin to promote cell adhesion on the sample surface. Therefore, the microtube samples were immersed overnight in a solution of octadecanylphosphonic acid (50 μmol; Aldrich) in toluene (Sigma–Aldrich) and rinsed with toluene, acetone (Technic France), and deionized water. To enable the cell culturing on the microtube samples, the cover glasses were glued to 3.5 cm plastic petri dishes with a 1.4 cm hole in the bottom (MatTek Corporation) using a two-components glue (picodent twinsil) before incubating the microtube structures with a 1× DPBS solution (Gibco) containing *N*-(3-dimethylaminopropyl)-*N*′-ethylcambodiimide hydrochloride (0.1 M, Sigma–Aldrich), *N*-hydroxylsulfosuccinimide (0.025 M; Aldrich), and fibronectin (0.02 mg $mL^{-1}$; Sigma) for 4 h at 37 °C. The microtube samples were carefully rinsed with 1× DPBS solution and stored at 4 °C until used.

## Cell Culture

Human osteosarcoma U2OS GFP-53BP1 cells have previously been described and were subcultured according to standard adherent mammalian tissue culture protocols.[31] They were grown in high-glucose DMEM (Sigma–Aldrich) supplemented with FBS (10%, Sigma–Aldrich), pyruvate ($1 \times 10^{-3}$ M, Gibco), penicillin (100 U $mL^{-1}$, Gibco), streptomycin (100 μg $mL^{-1}$, Gibco), and geneticin (0.5 mg $mL^{-1}$, Gibco) and were maintained in a humidified incubator (37 °C, 5% $CO_2$). For the experiments, the cells were detached using trypsin–EDTA solution (0.25%; Sigma) and resuspended in fresh medium for seeding on the microtube samples. To each 3.5 cm Petridish, $10^6$ cells in 3 mL medium were carefully added and allowed to settle before growing them for 2 more days in the humidified incubator to yield a nearly confluent monolayer. For the live-cell imaging experiments, the cell culture medium was exchanged to 3 mL of prewarmed phenolred free medium (constituents as listed above).

## Immunocytochemistry

Cells were fixed with 2% paraformaldehyde (Sigma–Aldrich) in DPBS for 15 min, rinsed once with DPBS, and permeabilized with 0.1% Triton X-100 in DPBS for 15 min. After washing three times with DPBS for 5 min each and removal of the liquid, a small drop of 4′, 6-Diamidin-2-phenylindol (DAPI, Invitrogen) containing mounting medium (Vector Laboratories) was applied and a 1.3-mm round coverslip (VWR) carefully placed on top of the microtube sample. The edges were sealed with conventional nail polish and the sample was stored at 4 °C until being imaged.

## Imaging and Analysis

Optical images of the fixed samples were taken with a Zeiss LSM 700 inverse confocal laser scanning microscope (40× objective, water immersion, NA = 1.2) employing the software ZEN 2010. Live-cell imaging was performed using a Zeiss Axio Observer. Z1 inverse microscope equipped with a 37 °C heated stage and $CO_2$ chamber (40× objective, oil immersion, NA = 1.1). The software Axio Vision Rel. 4.8 (Carl Zeiss, Inc.) was used for the image acquisition. The acquired images and image series were processed and analyzed with

Fiji (image processing package, distribution of ImageJ). The particle analyzer function was used to quantify the number of DNA damage foci in each cell nucleus (minimal focus size: 0.1 $\mu m^2$). Data are presented as mean ± standard deviation.

## Supplementary Material

Refer to Web version on PubMed Central for supplementary material.

## Acknowledgments

The authors thank the Gurdon Institute Imaging facility, especially Nicola Lawrence and Richard Butler, for support in image acquisition and analysis and the Biotec Light Microscopy Facility for training for the LSM700 microscope. The authors appreciate the design of Figure 1a by Dr. R. Träger. The results leading to this work have been financially supported by the Volkswagen Foundation (86 362) and the European Research Council (ERC) for Starting Grant “Lab-in-a-tube and Nanorobotics biosensors; LT-NRBS” [no. 311529]. C.K.S. acknowledges funding by a FEBS Return-to-Europe fellowship. Research in the SPJ laboratory is funded by Cancer Research UK, the ERC, and the European Community Seventh Framework Programme (DDResponse) with core infrastructure provided by Cancer Research UK and the Wellcome Trust.

## References

[1]. Folkman J, Moscona A. Nature. 1978; 273:345. [PubMed: 661946]

[2]. Singhvi R, Kumar A, Lopez GP, Stephanopoulos GN, Wang DI, Whitesides GM, Ingber DE. Science. 1994; 264:696. [PubMed: 8171320]

[3]. Thery M, Racine V, Pepin A, Piel M, Chen Y, Sibarita J-B, Bornens M. Nat. Cell Biol. 2005; 7:947. [PubMed: 16179950]

[4]. Chen CS, Mrksich M, Huang S, Whitesides GM, Ingber DE. Science. 1997; 276:1425. [PubMed: 9162012]

[5]. Yim EKF, Pang SW, Leong KW. Exp. Cell Res. 2007; 313:1820. [PubMed: 17428465]

[6]. Lee MR, Kwon KW, Jung H, Kim HN, Suh KY, Kim K, Kim KS. Biomaterials. 2010; 31:4360. [PubMed: 20202681]

[7]. Chalut KJ, Kulangara K, Giacomelli MG, Wax A, Leong KW. Soft Mater. 2010; 6:1675.

[8]. Thomas CH, Collier JH, Sfeir CS, Healy KE. Proc. Natl. Acad. Sci. 2002; 99:1972. [PubMed: 11842191]

[9]. Vogel V, Sheetz M. Nat. Rev. Mol. Cell Biol. 2006; 7:265. [PubMed: 16607289]

[10]. Lee J, Cuddihy MJ, Kotov NA. Tissue Eng. Part B. 2008; 14:61.

[11]. Santos E, Hernández RM, Pedraz JL, Orive G. Trends Biotechnol. 2012; 30:331. [PubMed: 22560988]

[12]. Tay CY, Irvine SA, Boey FYC, Tan LP, Venkatraman S. Small. 2011; 7:1361. [PubMed: 21538867]

[13]. Cukierman E, Pankov R, Stevens DR, Yamada KM. Science. 2001; 294:1708. [PubMed: 11721053]

[14]. Ingber DE. FASEB J. 2006; 20:811. [PubMed: 16675838]

[15]. McNamara LE, Burchmore R, Riehle MO, Herzyk P, Biggs MJ, Wilkinson CD, Curtis AS, Dalby MJ. Biomaterials. 2012; 33:2835. [PubMed: 22248989]

[16]. Khademhosseini A, Langer R, Borenstein J, Vacanti JP. Proc. Natl. Acad. Sci. 2006; 103:2480. [PubMed: 16477028]

[17]. Baker BM, Chen CS. J. Cell Sci. 2012; 125:3015. [PubMed: 22797912]

[18]. Soh S, Kandere-Grzybowska K, Mahmud G, Huda S, Patashinski AZ, Grzybowski BA. Adv. Mater. 2012; 24:5719. [PubMed: 22886834]

[19]. Ochsner M, Dusseiller MR, Grandin HM, Luna-Morris S, Textor M, Vogel V, Smith ML. Lab Chip. 2007; 7:1074. [PubMed: 17653351]

[20]. Dusseiller M, Smith M, Vogel V, Textor M. Biointerphases. 2006; 1:P1. [PubMed: 20408607]

[21]. Dahl DN, Ribeiro AJS, Lammerding J. Circ. Res. 2008; 102:1307. [PubMed: 18535268]
[22]. Lelièvre SA, Weaver VM, Nickerson JA, Larabell CA, Bhaumik A, Petersen OW, Bissell MJ. Proc. Natl. Acad. Sci. 1998; 95:14711. [PubMed: 9843954]
[23]. Le Berre M, Aubertin J, Piel M. Integr. Biol. 2012; 4:1406.
[24]. Mei YF, Huang G, Solovev AA, Ureña EB, Mönch I, Ding F, Reindl T, Fu RKY, Chu PK, Schmidt OG. Adv. Mater. 2008; 20:4085.
[25]. Huang GS, Mei Y, Thurmer DJ, Coric E, Schmidt OG. Lab Chip. 2009; 9:263. [PubMed: 19107283]
[26]. Smith EJ, Xi W, Makarov D, Mönch I, Harazim S, Quiñones VAB, Schmidt CK, Mei Y, Sanchez S, Schmidt OG. Lab Chip. 2012; 12:1917. [PubMed: 22437345]
[27]. Schulze S, Huang G, Krause M, Aubyn D, Bolaños Quiñones VA, Schmidt CK, Mei Y, Schmidt OG. Adv. Eng. Mater. 2010; 12:B558.
[28]. Xi W, Schmidt CK, Sanchez S, Gracias DH, Carazo-Salas RE, Jackson S, Schmidt OG. Nano Lett. 2014 DOI 10.1021/nl4042565.
[29]. Harazim SM, Xi W, Schmidt CK, Sanchez S, Schmidt OG. J. Mater. Chem. 2012; 22:2878.
[30]. Crissman HA, Steinkamp JA. J. Cell Biol. 1973; 59:766. [PubMed: 4128323]
[31]. Friedl P, Wolf K, Lammerding J. Curr. Opin. Cell Biol. 2011; 23:55. [PubMed: 21109415]
[32]. Galanty Y, Belotserkovskaya R, Coates J, Polo S, Miller KM, Jackson SP. Nature. 2009; 462:7275.
[33]. Schultz LB, Chehab NH, Malikzay A, Halazonetis TD. J. Cell Biol. 2000; 151:1381. [PubMed: 11134068]
[34]. Dahl KN, Booth-Gauthier EA, Ladoux B. J. Biomech. 2010; 43:2. [PubMed: 19804886]
[35]. Guilak F. J. Biomech. 1995; 28:1529. [PubMed: 8666592]
[36]. Dewey CF Jr. Bussolari SR, Gimbrone MA Jr. Davies PF. J. Biomech. Eng. 1981; 103:177. [PubMed: 7278196]
[37]. Screen HRC, Lee DA, Bader DL, Shelton JC. Biorheology. 2003; 40:361. [PubMed: 12454427]

Europe PMC Funders Author Manuscripts

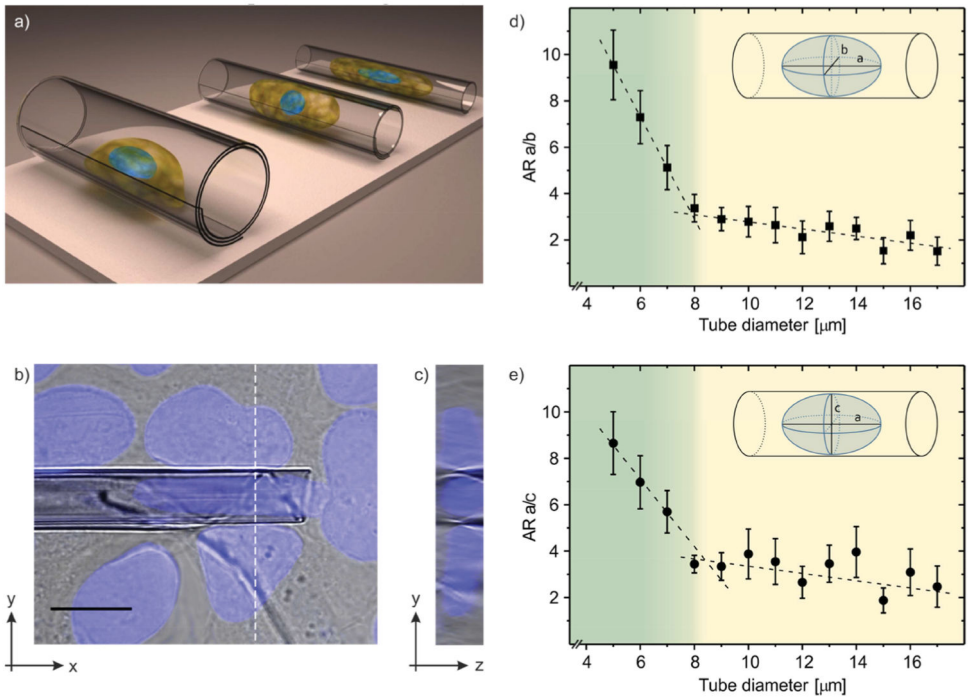


**Figure 1.**

Change of cell and nuclear morphology inside the microtube confinement. a) Schematic depicting the increasing elongation of a single confined cell with decreasing microtube diameter. b,c) Different views (merged bright-field/DAPI fluorescence images) of a U2OS cell that is confined inside a microtube of 6 μm diameter. The image in b) shows the top view, the dotted white line indicates a cut through the z-stack taken at the shown position. The resulting z-stack cross-section is indicated in c). The scale bar equals 10 μm. d) Aspect ratio (AR) of nucleus length *a* (along the microtube long axis) and width *b*. The inset schematic visualizes the nuclear dimensions. e) Aspect ratio of nucleus length *a* and height *c*. Shown error bars are based on the standard deviation of the respective values. A linear regression of the datasets reveals in both cases 8 μm as the critical tube diameter for a distinct manipulation of the nuclear dimensions *b* or *c*, respectively (for the absolute values of the nucleus dimensions please see Figure S1, Supporting Information).




Europe PMC Funders Author Manuscripts

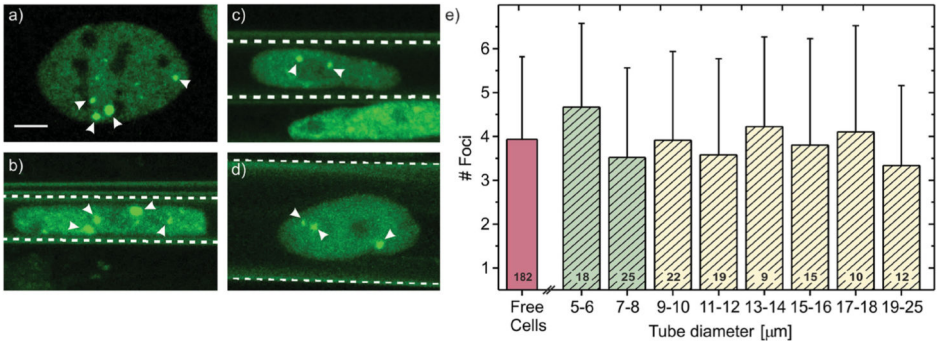


**Figure 2.**

Number of GFP-53BP1 foci in dependence on the diameter of the tubular confinement. a–d) Fluorescence images of GFP-labeled 53BP1 foci in U2OS cell nuclei. The cells are either grown on a) a 2D flat substrate (reference cell) or inside microtubes of b) 6 μm, c) 8 μm, and d) 18 μm diameter. White dashed lines indicate the positions of the microtube walls. Arrowheads point at 53BP1 foci, the scale bar equals 5 μm. e) Quantification of the amount of endogenously present foci of reference (red column) and confined cells (green, yellow columns: tube diameters smaller or larger than the critical threshold value of 8 μm (see Figure 1), respectively). Shown error bars are based on the standard deviation of the respective values, the number of evaluated cells is given at the base of each column.




Europe PMC Funders Author Manuscripts

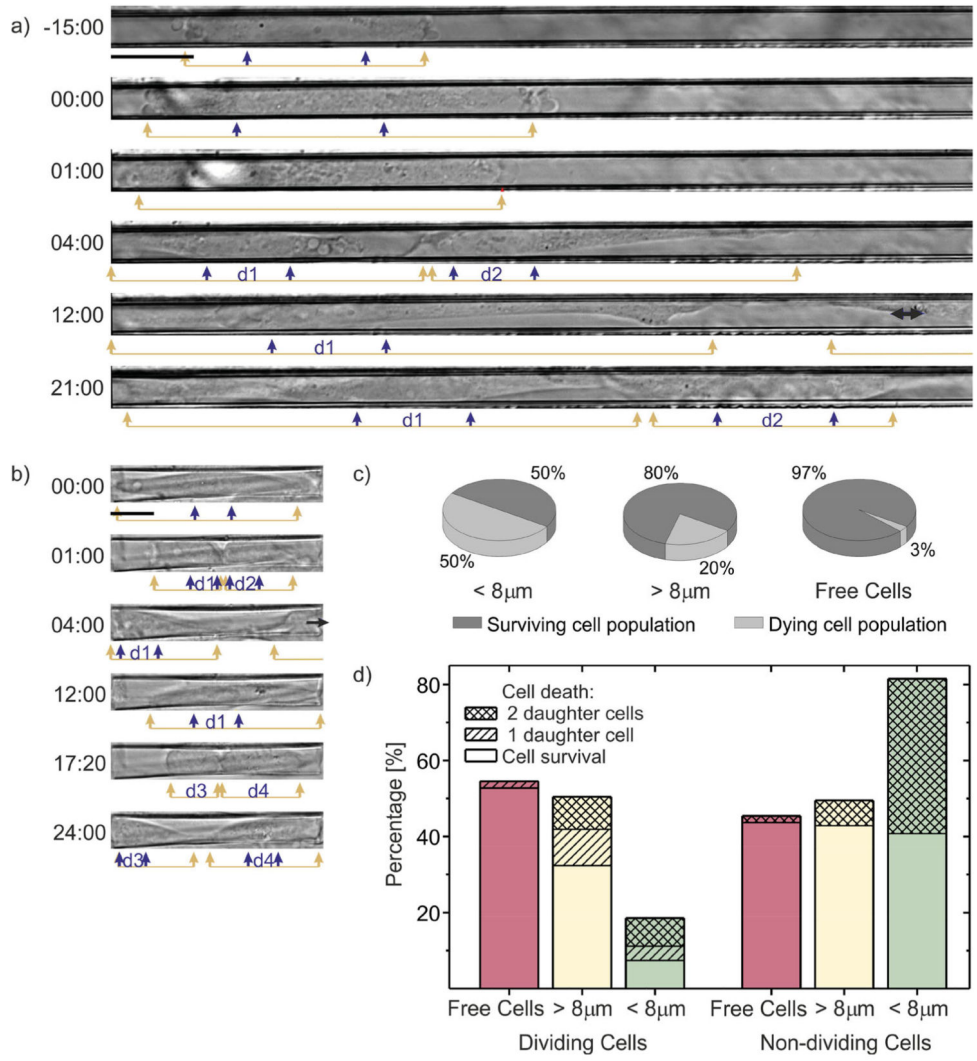


**Figure 3.**

Effects of spatial confinement on cell growth and proliferation. a,b) Live-cell imaging of U2OS cells growing inside a microtube of a) 6 µm and b) 13 µm diameter. Shown are bright-field images of characteristic time-points over a 35 to 47 h time course including a 15 h pre-mitotic imaging phase in a) and during a minimum 21 h observation period after the onset of mitosis (0 h). The time-points are indicated in h:min format to the left of each image, arrows indicate the outer rims of the cell nucleus (blue) and the whole cell (yellow). In mitotic cells, the nuclear confinement disappears due to the breakdown of the nuclear envelope. Horizontal black arrows indicate cells moving toward the outside of the tube. The arising daughter cells are named d1 and d2 for the first and d3 and d4 for the second generation. Scale bars equal 20 µm. In a) a distinct increase of the cell volume preceding the cell division is visible (compare −15:00 with 00:00). The two daughter cells (d1 and d2) arising from the division move along the microtube length but remain confined throughout the time course. One of the two arising daughter cells in (d2 in b) moves out of the tube (4 h), whereas the other one (d1) undergoes a second confined cell division (17 h 20 min, d3

and d4). c,d) Illustration of the cell fates of U2OS cells during a 20-h period of cell growth inside microtubes with diameters either smaller than the critical value of 8 μm (green colouring; $n = 27$) or above (yellow coloring; $n = 105$) in comparison to the fate of unconfined reference cells (red coloring; $n = 55$). In c) the overall survival of the cells during the observation period is depicted. In d) it is further discriminated between the cells that divide or show no cell division. Any arising daughter cells were monitored for an additional minimum observation time of 3.5 h after mitosis.



Europe PMC Funders Author Manuscripts